Enhanced efficiency in double junction polymer

Moet, D. J. D.; de Bruyn, P.; Kotlarski, J. D.; Blom, P. W. M.

Published in:
Organic Electronics

DOI:
10.1016/j.orgel.2010.08.010

Publication date:
2010

Organic Electronics 11 (2010) 1821–1827

Contents lists available at ScienceDirect

Organic Electronics

journal homepage: www.elsevier.com/locate/orgel

Enhanced efficiency in double junction polymer:fullerene solar cells

D.J.D. Moet [a,*], P. de Bruyn [a,b], J.D. Kotlarski [a], P.W.M. Blom [a,c]

[a] Zernike Institute for Advanced Materials, University of Groningen, Nijenborgh 4, 9747 AG Groningen, The Netherlands
[b] Dutch Polymer Institute, P.O. Box 902, 5600 AX Eindhoven, The Netherlands
[c] Holst Centre, High Tech Campus 31, 5605 KN Eindhoven, The Netherlands

ARTICLE INFO

Article history:
Received 5 July 2010
Received in revised form 23 July 2010
Accepted 12 August 2010
Available online 27 August 2010

Keywords:
Polymer
Solar cells
Tandem
PF10TBT
Optoelectronic modeling

ABSTRACT

Polymer solar cells based on the polyfluorene copolymer poly[9,9-didecanefluorene-alt-(bis-thienylene) benzothiadiazole] (PF10TBT) and the fullerene derivative [6,6]-phenyl C_{61}-butyric acid methyl ester (PCBM) exhibit a power conversion efficiency of 4%. However, the optimum thickness of the photoactive layer is only 80 nm, such that these solar cells absorb only half of the photons available in their absorption bandwidth. Thicker cells are subject to electronic losses due to space charge effects and recombination. We demonstrate both from simulations and experiments that the optical and electronic losses can be decoupled in a double junction solar cell. For the PF10TBT:PCBM blend, the integration of two thin cells in a double junction device leads to an enhancement of the measured power conversion efficiency with 13% up to a value of 4.5%.

1. Introduction

The active layer of the most efficient polymer solar cells to date consists of a bulk heterojunction (BHJ) of a conjugated polymer with the buckminster fullerene derivative [6,6]-phenyl C_{61}-butyric acid methyl ester (PCBM). Such a bulk heterojunction is characterized by nanoscale intermixing of the electron donor and acceptor materials in order to maximize their cross-sectional area [1]. Compared to inorganic solar cells, thin film polymer devices produce high photovoltages. However, the power conversion efficiency is limited by a relatively low photocurrent as a result of a higher bandgap and narrower absorption bandwidth. Efforts to increase the efficiency are therefore primarily focused on the harvesting of more photons.

The most direct way to increase absorption is increasing the thickness of the photoactive layer. However, in many polymer:fullerene systems the combined effects of charge carrier recombination and the formation of space charge reduce the fill factor and consequently the overall device efficiency of thick cells [2]. In a BHJ solar cell the reflective back electrode introduces optical interference effects inside the photoactive layer between incoming and reflected light [3]. Therefore, it has been suggested that the photocurrent can be increased by introducing an optical spacer that enhances light absorption in thin polymer solar cells by redistributing the optical electric field [4,5]. However, the spacer effect is only beneficial if the BHJ film thickness does not coincide with a local maximum of optical power dissipation [6].

Alternatively, the optical properties of the photoactive materials can be tuned. Promising results have been reported for solar cells in which narrow bandgap polymers were introduced in order to absorb low-energy photons [7–9]. The electron-accepting material can be modified as well: substitution of PCBM with its more strongly absorbing C_{70}-analogue generally results in a larger contribution to the photocurrent [10]. A further improvement of the spectral coverage of the solar irradiance spectrum can be realized by incorporation of multiple heterojunctions with complementary absorption spectra in a tandem solar cell [11–13].

In this paper we present an alternative approach to improve the performance of thin film polymer photovoltaics. As a model system we use polymer solar cells based on the

* Corresponding author.
E-mail address: d.j.d.moet@rug.nl (D.J.D. Moet).

1566-1199/$ - see front matter © 2010 Elsevier B.V. All rights reserved.
doi:10.1016/j.orgel.2010.08.010

polyfluorene copolymer poly[9,9-didecanefluorene-alt-(bis-thienylene) benzothiadiazole] (PF10TBT) and PCBM with a power conversion efficiency of 4%. An efficiency increase of 13% is realized by combining two optimized PF10TBT:PCBM solar cells in one double junction device, without any change to the constituents of the photoactive layer. The approach concurrently utilizes the enhanced absorption of thick films and the superior electronic performance of thin films.

2. Experimental

2.1. Device fabrication

ITO patterned glass substrates were thoroughly cleaned with soap water, acetone, propanol and a UV ozone treatment before application of a layer of PEDOT:PSS (Clevios VP AI4083 SG, H.C. Starck). PF10TBT (TNO, M_w = 1.9 $\times$ 10^5 g/mol, PDI = 3.5) and PCBM (Solenne) were used as received. Photoactive layers were spin coated under ambient conditions from hot (90 °C) chlorobenzene solutions of PF10TBT:PCBM in a 1:4 weight ratio and capped with a 1 nm LiF/100 nm Al cathode. For the middle electrode of double junction devices, ZnO nanoparticles with a diameter of 5–10 nm were synthesized in methanol via hydrolysis and condensation of zinc acetate dihydrate by KOH, as described elsewhere [14,15]. After centrifugation, the ZnO gels were dispersed in acetone [16], followed by sonication and filtration. The acidity of PEDOT:PSS (Clevios PH500, H.C. Starck) was tuned by addition of a 1:8 dilution of 2-dimethylaminoethanol in water [17]. Nafion perfluorinated resin solution (5 wt% in a mixture of lower aliphatic alcohols and water, Aldrich) was diluted 1:20 with ethanol before spin coating at high rpm on top of pH-modified PEDOT:PSS layers in a nitrogen-flushed compartment under ambient atmosphere.

2.2. Characterization

Current–voltage characteristics were recorded with a Keithley 2400 SourceMeter. The results of Fig. 1 were recorded under illumination from a Steuernagel SolarConstant 1200, producing white light with an intensity of 1.3 kW/m^2. The light intensity was determined by (a) comparison of the measured J_{sc} with the expected short-circuit current density as calculated from the convolution of the spectral responsivity curve with the AM1.5 global reference spectrum, taking into account the linear dependence of J_{sc} on light intensity and (b) the deviation of the setpoint of a multicrystalline silicon reference cell from the value determined using accurate mismatch correction [18]. The same lamp was used for the measurements of Fig. 6, using spectral mismatch correction (M = 1.40) and a GG385 filter, resulting in a light intensity equivalent to 0.9 sun. Contributions to the photocurrent from regions outside the anode/cathode overlap area were eliminated using illumination masks with slightly smaller apertures. Incident photon to current conversion efficiency (IPCE) spectra were measured from 400 to 1100 nm using a custom-built setup comprising a 50 W quartz tungsten halogen lamp, 28 narrow band-pass interference filters, a transimpedance amplifier and a lock-in amplifier. The spectral response was measured relative to that of a calibrated monocrystal-

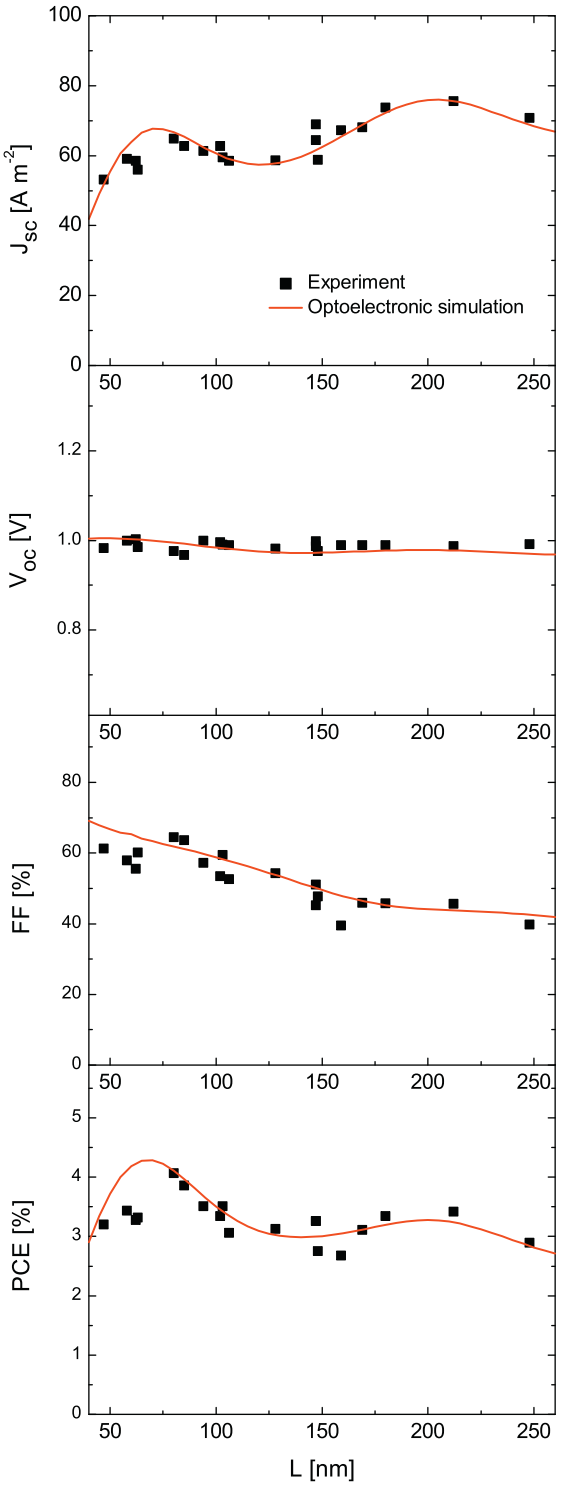

Fig. 1. Squares: experimental photovoltaic data of PF10TBT:PCBM solar cells with varying active layer thickness. The lines denote the result of the combined optoelectronic simulation.

line silicon photodiode (Newport 818-SL). Layer thickness measurements were done with a Veeco Dektak 6 M or 150 profilometer. Optical absorbance was measured with a Perkin–Elmer Lambda 900 spectrophotometer.

3. Results and discussion

3.1. Single junction solar cells

The efficiency of PF10TBT:PCBM solar cells is known to increase with the molecular weight of the polymer. This is caused by a reduced recombination rate of bound electron–hole pairs at high molecular weights, which leads to more efficient generation of free charges [19]. Therefore, the solar cells studied here are based on bulk heterojunctions of PCBM and high molecular weight PF10TBT. The donor/acceptor weight ratio was fixed to the optimum of 1:4 and all devices were processed from hot chlorobenzene solutions.

The variation of the short-circuit current density J_{sc}, open-circuit voltage V_{oc}, fill factor FF and power conversion efficiency PCE with photoactive layer thickness L is displayed in Fig. 1. Each data point (squares) represents the average of three or more current density–voltage (J–V) measurements. The values of J_{sc} and PCE were corrected for spectral mismatch of the lamp with the solar spectrum (see Section 2.2). Noticeable is the oscillatory behavior of J_{sc}, characterized by maxima at L = 80 nm and L = 210 nm. Thicker cells clearly absorb more light as J_{sc} is highest for L > 150 nm. However, since the open-circuit voltage is virtually independent of layer thickness and the fill factor strongly decreases with increasing L, the overall experimental PCE reaches its highest value of 4.0% already at L = 80 nm.

Next, we use combined optoelectronic modeling to gain insight in the major limitations of PF10TBT:PCBM solar cells of varying thickness. In order to describe the experimental results, we use an optical model based on the transfer matrix formalism in combination with a numerical electronic device model [20].

3.1.1. Optical simulations

Most conjugated polymers exhibit strong absorption with a high peak absorption coefficient [21]. As a result, layers as thin as several hundreds of nanometers can effectively absorb most solar photons with energy higher than the bandgap of the polymer. Since the wavelength of the incoming light is of a similar length scale and the back electrode in polymer solar cells is usually highly reflective, optical interference effects have to be taken into account in the description of the photocurrent of such devices [3].

As input for the optical model, the index of refraction n, extinction coefficient k and thickness of each layer in the device architecture are used. The optical constants were determined previously using variable-angle spectroscopic ellipsometry [19]. The light intensity $I(\lambda,x)$ is calculated for each wavelength and position inside the entire layer stack, taking into account the optical properties of each layer as well as the interference of light that is incident on the device (AM1.5G, 1000 W/m^2) with light that is reflected by the back electrode. The exciton generation rate at each position in the polymer:fullerene layer is given by the convolution of the local spectral photon flux and the absorption spectrum of the active layer [20]. In the calculation the relevant wavelength range is discretized at exponentially equidistant values λ_i and the integral is consequently replaced by a summation:

$$G(x) = \sum_i \frac{4\pi k(\lambda_i)}{hc} I(\lambda_i, x)\Delta\lambda_i \quad (1)$$

where $G(x)$ is the exciton generation rate at position x, h is Planck's constant, c is the speed of light and $I(\lambda_i,x)$ is the light intensity at wavelength λ_i and position x. The exciton generation profiles $G(x)$ are used below as an input for the electronic device model. A final integration of $G(x)$ over the position in the device gives the total generation rate G_{tot} of excitons inside the photoactive layer.

By definition, the amount of absorbed photons is equal to the amount of photogenerated excitons G_{tot}. For the AM1.5G reference spectrum, the number of *incident* photons with wavelengths within the effective absorption bandwidth of PF10TBT:PCBM layers, i.e., 300 < λ < 650 nm, is $N_{ph} = 1.05 \times 10^{21}$ m^{-2} s^{-1}. A measure of the absorption efficiency is now given by the ratio of G_{tot} to N_{ph}, which is plotted versus layer thickness in Fig. 2 (solid line). At L = 80 nm, which is the point of the first maximum of the experimental J_{sc}, only 48% of the available photons are absorbed. Poor light absorption thus strongly limits the current these thin PF10TBT:PCBM solar cells can produce. As expected, this conclusion is not altered by the introduction of an optical spacer in the form of a thin ZnO layer between the active layer and the cathode, since the incoupling of light is already optimal, giving a local maximum of the dissipated optical power at L = 80 nm. At the other local maximum of the experimental short-circuit current density, L = 210 nm, two-thirds of the available photons are absorbed. This shows that the available light can be used more efficiently in order to increase cell performance, without reducing the bandgap of the polymer.

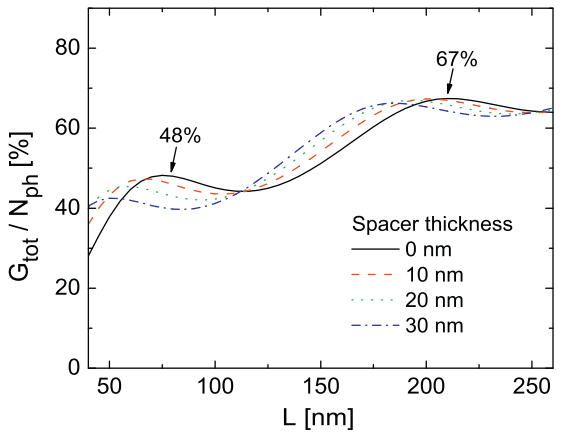

Fig. 2. Ratio of photogenerated excitons G_{tot} to the amount of photons N_{ph} with wavelength between 300 and 650 nm as a function of layer thickness. The lines denote different optical spacer thicknesses as indicated in the legend.

3.1.2. Electronic simulations

In polymer:fullerene solar cells, photogeneration of excitons is followed by diffusion of the excitons towards a donor–acceptor interface, charge transfer at the interface, dissociation of the resulting bound electron–hole (e–h) pair and charge carrier transport to and extraction at separate electrodes. Each of these processes generally introduces electrical losses that reduce the amount of extracted charges. The cumulative effect of these losses at short-circuit conditions is represented in the internal quantum efficiency, defined as the number of electrons in an external circuit per absorbed photon, or IQE = J_{sc}/qG_{tot}, where q is the elementary charge. The IQE can thus directly be determined from the measured J_{sc} (Fig. 1) and calculated G_{tot} (Fig. 2). In Fig. 3, the resulting IQE is plotted versus photoactive layer thickness. Approximately 80% of the absorbed photons contribute to the photocurrent in thin cells. For thicker layers this fraction decreases monotonically to around 70%, which is in good agreement with previously reported results [22].

Next, the current–voltage characteristics are simulated for each L in the range of experimental layer thicknesses. Here we use our numerical device model that includes drift and diffusion of charge carriers, a temperature- and field-dependent generation rate of free carriers, bimolecular recombination and the effect of space charge on the electric field in the device [23]. Ultrafast electron transfer from the photoexcited polymer to PCBM is assumed to occur with unity quantum yield, i.e., each exciton generates a bound e–h pair at an interface of donor and acceptor molecules. The dissociation rate of bound pairs into free carriers is described by Onsager–Braun theory [24,25], using an initial e–h separation distance a with a Gaussian distribution in energy and a bound pair decay rate k_f to parameterize the dependence of the dissociation probability P on electric field and temperature. Recombination of free carriers is assumed to be of the Langevin type, with a recombination constant dominated by the slowest carrier [26], and results in a bound pair that can either dissociate again or decay to the ground state. Other relevant parameters are the electron and hole mobilities μ_e and μ_h, the spatially averaged relative dielectric constant ε_r and the effective energy gap E_{gap} between the highest occupied molecular orbital (HOMO) energy of the donor and the lowest unoccupied molecular orbital (LUMO) energy of the acceptor.

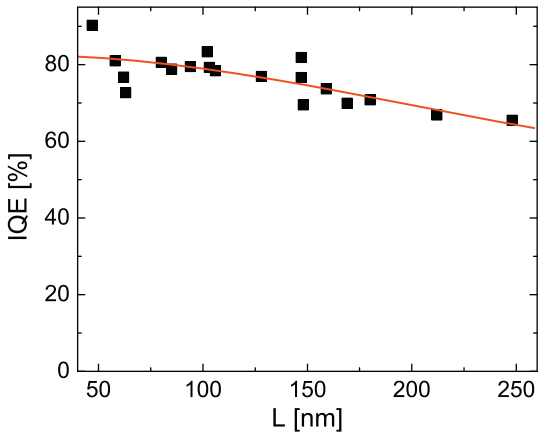

Fig. 3. The internal quantum efficiency IQE = J_{sc}/qG_{tot} versus photoactive layer thickness. The line serves as a guide to the eye.

The exciton generation profiles obtained by optical modeling are used as an input for the electronic model. The values that were used for the parameters in the electronic model are in excellent agreement with those previously derived for high molecular weight PF10TBT:PCBM cells [19] and are summarized in Table 1. In Fig. 1, the results of the optoelectronic simulations are depicted by the solid lines. Clearly, the oscillations of the short-circuit current density and power conversion efficiency with thickness are reproduced, as well as the strongly decreasing fill factor. The simulations indicate an optimal thickness of around 70 nm, which is close to the experimental value of 80 nm. The ratio of the amount of excitons that are lost due to quenching at the electrodes to the total amount of photogenerated excitons is large in very thin cells. As this quenching effect is not incorporated in the model, the calculations slightly overestimate the fill factor and short-circuit current in thin cells and, consequently, the predicted value of the maximum PCE of 4.3% is somewhat higher than the optimal experimental value.

Based on the optical simulations of Section 3.1.1, a relative increase of 40% in J_{sc} would be expected for a 210 nm thick cell compared to the 80 nm thick device. As can be seen in Fig. 1, enhanced absorption in thicker cells does indeed enable the extraction of a higher current. However, limited by the combined effects of space charge and recombination, the short-circuit current at L = 210 nm is only 16% higher than that at L = 80 nm. The same limitation causes the fill factor to drop considerably, resulting in a reduction of the PCE to 3.2%.

This clearly demonstrates that the increased absorption in thick cells is opposed by less favorable electronic properties. As a result the processing window for optimized solar cells is limited to thin layers. In the following section, the interlocking of optics and electronics is reduced by using double junction solar cells consisting of two optimized thin layer devices.

3.2. Double junction solar cells

Multijunction solar cells are generally used to compensate for the relatively narrow absorption bandwidth of conjugated polymers. By inclusion of a second bulk heterojunction with a lower optical bandgap, photon harvesting

Table 1
Overview of the model parameters used in the simulations.

Parameter	Symbol	Value
Bandgap	E_{gap}	1.37 eV
Electron mobility	μ_e	1×10^{-7} m^2 V^{-1} s^{-1}
Hole mobility	μ_h	6×10^{-9} m^2 V^{-1} s^{-1}
Effective density of states	N_c	2.5×10^{25} m^{-3}
Relative dielectric constant	ε_r	3.6
Initial e–h pair distance	a	2.2 nm
e–h Pair decay rate	k_f	5×10^5 s^{-1}

can be extended from the visible towards the near infrared. However, as discussed above, thin solar cells based on high bandgap materials fail to absorb a lot of photons with sufficient energy. In this section we therefore choose to investigate the possibility to enhance absorption of these high energy photons.

The photovoltaic properties of a multijunction solar cell depend on the method of interconnection of the subcells. A polymer tandem cell containing two subcells in a parallel configuration is feasible and is generally capable of producing higher currents [27]. However, charges need to be extracted at the middle electrode, which should consequently be based on materials with high sheet conductivity, such as metals. So far this has been incompatible with processing from solution. A much more practical approach is the series-connected multijunction, in which an increase in the amount of absorbed photons is utilized to deliver a higher photovoltage rather than a high current. As conduction now mainly occurs perpendicular to the interface, less conductive materials such as conjugated polymers and metal oxides are suitable candidates for the interlayer as well.

Here, we employ a previously reported device architecture in which the two subcells are connected in series by a composite middle electrode of ZnO nanoparticles and pH-modified PEDOT:PSS [16]. For practical reasons, the thicknesses of these layers are fixed to 20 and 30 nm, respectively.

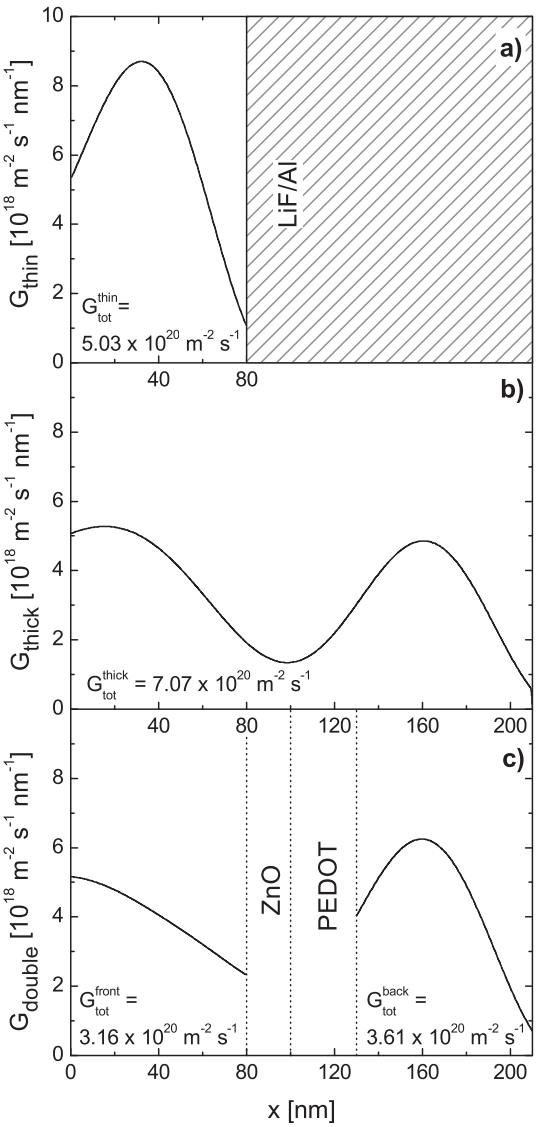

Fig. 4. Calculated exciton generation rate profiles plotted versus the position x in (a) a thin, (b) a thick and (c) a double junction solar cell. The total (integrated) exciton generation rate G_{tot} for each profile is indicated in the relevant figure panel.

3.2.1. Simulations

As a reference, we first take a step back to examine the exciton generation profiles of a thin and a thick device, as shown in Fig. 4a and b. Again we consider the layer thicknesses at the maxima of the experimental J_{sc} and PCE, i.e., L = 80 nm and L = 210 nm. Position x = 0 corresponds to the interface of PEDOT:PSS with the photoactive layer and the cathode is located at $x = L$. The light can thus be considered incident from the left side of the figure. As expected, both profiles show excellent incoupling of the incident light. Furthermore, as discussed above, the ratio of the total exciton generation rates amounts to $G_{tot}^{thick}/G_{tot}^{thin} = 1.40$, which means that the thick cell absorbs 40% more photons than the thin one.

In Fig. 4c, the exciton generation profiles inside the two subcells of a double junction device are plotted. As a one-to-one extension of the optimized single layer cell, the tandem device is chosen to incorporate two thin PF10TBT:PCBM cells of 80 nm thickness. These are separated by a ZnO cathode (20 nm) for the front cell and PEDOT:PSS anode (30 nm) for the back cell, which results in a

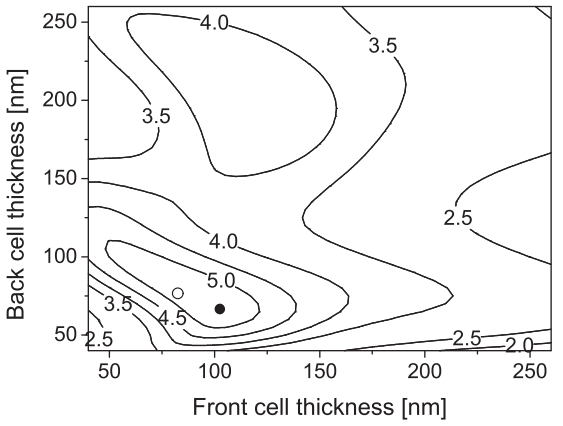

Fig. 5. Layer thickness dependence of the efficiency of a double junction device (labels) as predicted by combined optoelectronic simulations. For each combination of layer thicknesses, the exciton generation profiles inside the subcells were calculated and used as an input for our numerical device model. The J–V curves of tandem cells were constructed from the subcell characteristics [28]. The symbols indicate the optimal combination of subcell thicknesses (filled circle) and the case of two 80 nm thick subcells (open circle).

total device thickness of 210 nm. It can be seen that the shape of the generation profile in the back cell is similar to the one of the single thin layer because it is closest to the reflective cathode. As expected the magnitude of $G(x)$ in the back cell is lower than in the single layer thin cell due to optical interference effects and absorption in the front cell. However, *in total* the double junction absorbs more photons, in fact nearly as much (96%) as the 210 nm thick single layer device. In contrast, a single layer of 160 nm thickness absorbs only 81% of G_{tot}^{thick}. In other words, the double junction device absorbs more photons per nanometer of photoactive material than thick single layer cells due to the presence of the transparent middle electrode.

In order to predict the photovoltaic properties of the double junction device, we consider the general properties of a series-connected tandem cell. First, since each subcell is as thick as the thin single layer device and based on the same donor–acceptor system, it is reasoned that they will exhibit a similar IQE, FF and V_{oc}. Similarly, this also means that the FF of the double junction device will be the same as the FF of the subcells whereas its V_{oc} will be twice as large. Of the two subcells in the particular device considered in Fig. 4c, the front cell produces the least amount of excitons ($G_{tot}^{front} < G_{tot}^{back}$). As the IQE is invariant, this subcell will be current-limiting under short-circuit conditions and thus determine J_{sc} of the double junction device. Then, the ratio of the short-circuit current densities of the double junction cell and the thin, optimized single layer cell is close to $G_{tot}^{front}/G_{tot}^{thin} = 0.63$. It is thus predicted that a stack of two thin cells produces a J_{sc} that amounts to ca. 63% of the value for the single layer device. Combined with a doubled V_{oc} and an unchanged FF, an ideal double junction device is expected to have a 26% higher efficiency than the optimized single layer device.

The efficiency increase that is obtained with the use of a double junction structure can be enlarged slightly when the layer thicknesses of the subcells are chosen such that light absorption is more balanced. As indicated in Fig. 5, combined optoelectronic simulations of double junction devices predict that the highest performance would be expected for a device with a front cell thickness of 100 nm and a back cell thickness of 70 nm. However, since a more straightforward double junction device with two 80 nm thick subcells should perform much better than a single junction cell as well, we will employ this structure in the experimental section below.

3.2.2. Comparison with experiment

To determine the advantageous effect of a double junction structure on the performance of a real device, a slight modification to the anode of the back cell was necessary. The work function of pH-modified PEDOT:PSS is lower than that of unmodified PEDOT:PSS, which would result in a reduction of the open-circuit voltage of the back cell. To prevent this, an ultrathin layer of a perfluorinated ionomer was spin coated on the middle electrode [17]. Since the perfluorinated ionomer layer is presumably only a few monolayers thick, it is not expected to affect the optical properties of the layer stack. Fig. 6 shows the measured and simulated J–V curves of single and double junction cells with active layers of 80 nm thickness. At a light intensity of 0.9 sun, the experimental double junction device delivers a J_{sc} of 34.9 A/m^2 compared to 56.0 A/m^2 for the 80 nm thick single layer cell. The J_{sc} ratio thus amounts to 62%, which is in excellent agreement with the calculated value of 63%. At 1.92 V the V_{oc} of the double junction cell is very close to but slightly lower than the sum of the subcell voltages (1.94 V). Unfortunately, the fill factor shows a small drop as well, from 66% to 61%, which is most probably caused by an additional series resistance due to the thin insulating layer between the back photoactive layer and its anode. Nevertheless, the power conversion efficiency increases with 13% from 4.0% for the optimized single layer device to 4.5% for the double junction device. The decoupling of optical and electronic limitations thus clearly enables an enhancement of the photovoltaic performance. The working principle is therefore generic to all polymer:fullerene systems that show optimum performance at small layer thicknesses.

4. Conclusions

The photovoltaic properties of PF10TBT:PCBM solar cells are described with combined optoelectronic modeling to identify the processes that limit the power conversion

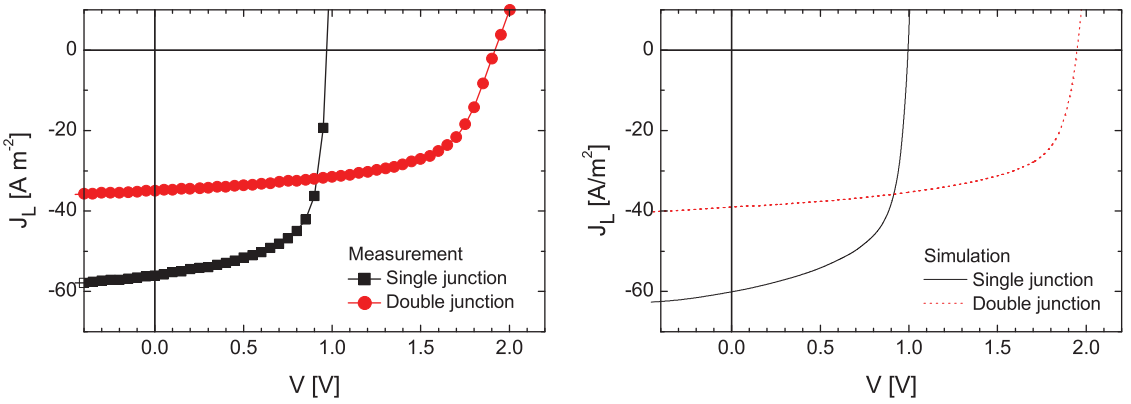

Fig. 6. Experimental (left) and calculated (right) current density versus voltage curves of a single and a double junction cell at a light intensity of 0.9 sun. The (sub)cells are all 80 nm thick.

efficiency. It is shown that 4%-efficient solar cells with an optimized layer thickness of 80 nm absorb only 48% of the photons that are available within the absorption bandwidth. Optical modeling reveals that this figure can be increased to 67% if the PF10TBT:PCBM layer is made 210 nm thick. However, a concurrent decrease in fill factor limits the efficiency of thick cells to 3.2%. It is shown that a double junction solar cell consisting of two optimized PF10TBT:PCBM layers absorbs photons more efficiently than thick single layer cells, as its structure disentangles the optical and electronic limitations. Simultaneously, the subcells have the high internal quantum efficiency and fill factor associated with thin cells. Overall, the power conversion efficiency is improved from 4.0% for an optimized single layer cell to 4.5% for the double junction device.

Acknowledgements

The authors thank J. Sweelssen and M.M. Koetse for the supply of PF10TBT and J. Harkema and F. van der Horst for technical assistance. This work was funded by Senter Novem via the EOS Long Term program ZOMER (EOS LT 03026) and partly supported by the Dutch Polymer Institute (DPI), Project DPI No. 660.

References

[1] G. Yu, J. Gao, J.C. Hummelen, F. Wudl, A.J. Heeger, Science 270 (1995) 1789.
[2] M. Lenes, L.J.A. Koster, V.D. Mihailetchi, P.W.M. Blom, Appl. Phys. Lett. 88 (2006) 243502.
[3] L.A.A. Pettersson, L.S. Roman, O. Inganäs, J. Appl. Phys. 86 (1999) 487.
[4] J.Y. Kim, S.H. Kim, H. Lee, K. Lee, W. Ma, X. Gong, A.J. Heeger, Adv. Mater. 18 (2006) 572.
[5] J. Gilot, I. Barbu, M.M. Wienk, R.A.J. Janssen, Appl. Phys. Lett. 91 (2007) 113520.
[6] B.V. Andersson, D.M. Huang, A.J. Moulé, O. Inganäs, Appl. Phys. Lett. 94 (2009) 043302.
[7] J. Peet, J.Y. Kim, N.E. Coates, W.L. Ma, D. Moses, A.J. Heeger, G.C. Bazan, Nat. Mater. 6 (2007) 497.
[8] M.M. Wienk, M. Turbiez, J. Gilot, R.A.J. Janssen, Adv. Mater. 20 (2008) 2556.
[9] R. Kroon, M. Lenes, J.C. Hummelen, P.W.M. Blom, B. de Boer, Polym. Rev. 48 (2008) 531.
[10] M.M. Wienk, J.M. Kroon, W.J.H. Verhees, J. Knol, J.C. Hummelen, P.A. van Hal, R.A.J. Janssen, Angew. Chem. Int. Ed. 42 (2003) 3371.
[11] A. Hadipour, B. de Boer, P.W.M. Blom, Adv. Funct. Mater. 18 (2008) 169.
[12] J. Gilot, M.M. Wienk, R.A.J. Janssen, Adv. Mater. 22 (2010) E67.
[13] J.Y. Kim, K. Lee, N.E. Coates, D. Moses, T. Nguyen, M. Dante, A.J. Heeger, Science 317 (2007) 222.
[14] C. Pacholski, A. Kornowski, H. Weller, Angew. Chem. Int. Ed. 41 (2002) 1188.
[15] W.J.E. Beek, M.M. Wienk, M. Kemerink, X. Yang, R.A.J. Janssen, J. Phys. Chem. B 109 (2005) 9505.
[16] J. Gilot, M.M. Wienk, R.A.J. Janssen, Appl. Phys. Lett. 90 (2007) 143512.
[17] D.J.D. Moet, P. de Bruyn, P.W.M. Blom, Appl. Phys. Lett. 96 (2010) 153504.
[18] J.M. Kroon, M.M. Wienk, W.J.H. Verhees, J.C. Hummelen, Thin Solid Films 403–404 (2002) 223.
[19] D.J.D. Moet, M. Lenes, J.D. Kotlarski, S.C. Veenstra, J. Sweelssen, M.M. Koetse, B. de Boer, P.W.M. Blom, Org. Electron. 10 (2009) 1275.
[20] J.D. Kotlarski, P.W.M. Blom, L.J.A. Koster, M. Lenes, L.H. Slooff, J. Appl. Phys. 103 (2008) 084502.
[21] K.M. Coakley, M.D. McGehee, Chem. Mater. 16 (2004) 4533.
[22] L.H. Slooff, S.C. Veenstra, J.M. Kroon, D.J.D. Moet, J. Sweelssen, M.M. Koetse, Appl. Phys. Lett. 90 (2007) 143506.
[23] L.J.A. Koster, E.C.P. Smits, V.D. Mihailetchi, P.W.M. Blom, Phys. Rev. B 72 (2005) 085205.
[24] C.L. Braun, J. Chem. Phys. 80 (1984) 4157.
[25] V.D. Mihailetchi, L.J.A. Koster, J.C. Hummelen, P.W.M. Blom, Phys. Rev. Lett. 93 (2004) 216601.
[26] L.J.A. Koster, V.D. Mihailetchi, P.W.M. Blom, Appl. Phys. Lett. 88 (2006) 052104.
[27] A. Hadipour, B. de Boer, P.W.M. Blom, J. Appl. Phys. 102 (2007) 074506.
[28] A. Hadipour, B. de Boer, P.W.M. Blom, Org. Electron. 9 (2008) 617.